

# Generalizing Complex/Hyper-complex Convolutions to Vector Map Convolutions

Chase J Gaudet  
cjg7182@louisiana.edu

Anthony S Maida  
maida@louisiana.edu

October 11, 2021

## Abstract

We show that the core reasons that complex and hypercomplex valued neural networks offer improvements over their real-valued counterparts is the weight sharing mechanism and treating multidimensional data as a single entity. Their algebra linearly combines the dimensions, making each dimension related to the others. However, both are constrained to a set number of dimensions, two for complex and four for quaternions. Here we introduce novel vector map convolutions which capture both of these properties provided by complex/hypercomplex convolutions, while dropping the unnatural dimensionality constraints they impose. This is achieved by introducing a system that mimics the unique linear combination of input dimensions, such as the Hamilton product for quaternions. We perform three experiments to show that these novel vector map convolutions seem to capture all the benefits of complex and hyper-complex networks, such as their ability to capture internal latent relations, while avoiding the dimensionality restriction.

## 1 Introduction

While the large majority of work in the area of machine learning (ML) has been done using real-valued models, recently there has been an increase in use of complex and hyper-complex models [24, 17]. These models have been shown to handle multidimensional data more effectively and require fewer parameters than their real-valued counterparts.

For tasks with two dimensional input vectors, complex-valued neural networks (CVNNs) are a natural choice. For example in audio signal processing the magnitude and phase of the signal can be encoded as a complex number. Since CVNNs treat the magnitude and phase as a single entity, a single activation captures their relationship as opposed to real-valued networks. CVNNs have been shown to outperform or match real-valued networks, while sometimes at a lower parameter count [25, 2]. However, most real world data has more than two dimensions such as color channels of images or anything in the realm of 3D space.

The quaternion number system extends the complex numbers. These hyper-complex numbers are composed of one real and three imaginary components making them ideal for three or four dimensional data. Quaternion neural networks (QNNs) have enjoyed a surge in recent research and show promising results [22, 3, 5, 14, 15, 18, 19, 16]. Quaternion networks have been shown to be effective at capturing relations within multidimensional data of four or fewer dimensions. For example the red, green, and blue color image channels for image processing networks needs to capture the cross channel relationships of these colors as they contain important information to support good generalization [12, 9]. Real-valued networks treat the color channels as independent entities unlike quaternion networks. Parcollet et al. [16] showed that a real-valued, encoder-decoder fails to reconstruct unseen color images due to it failing to capture local (color) and global (edges and shapes) features independently, while the quaternion encoder-decoder can do so. Their conclusion is that the Hamilton product of the quaternion algebra allows the quaternion network to encode the color relation since it treats the colors as a single entity. Another example is 3D spatial coordinates for robotic and human-pose estimation. Pavllo et al. [20] showed improvement on short-term prediction on the Human3.6M dataset using a network that encoded rotations as quaternions over Euler angles.

The prevailing view is that the main reason that these complex networks outperform real-valued networks is their underlying algebra which treats the multidimensional data as a single entity. This allows the complex networks to capture the relationships between the dimensions without the trade-off of learning global features. However, using complex or hyper-complex numbers limits the dimensions to either two for complex or four with quaternions. There are higher dimensional hyper-complex systems such as octonions at eight dimensions, but they are a non-associative algebra.

This paper considers a novel hypothesis that may explain the effectiveness of complex/hypercomplex networks. Their convolutional operations use a form of weight sharing not found in real-valued networks. It may be that this weight sharing alone is sufficient to explain the learning advantages described above. If the weight sharing, rather than the algebra, is the most important factor for the enhanced learning abilities, then it may be possible to drop the dimensionality constraints imposed by the complex/hypercomplex algebras. Therefore, the present paper proposes: 1) to create a system that mimics the concepts of complex and hyper-complex numbers for neural networks, which treats multidimensional input as a single entity and incorporates weight sharing, but is not constrained to certain dimensions<sup>1</sup>; 2) to increase their local learning capacity by introducing a learnable parameter inside the multidimensional dot product. Our experiments herein show that these novel vector map convolutions seem to capture all the benefits of complex and hyper-complex networks, while improving their ability to capture internal latent relations, and avoiding the dimensionality restriction.

## 2 Motivation for Vector Map Convolutions

Nearly all data used in machine learning is multidimensional and, to achieve good performance models, must both capture the local relations within the input features [23, 13], as well as non-local features, for example edges or shapes composed by a group of pixels. Complex and hyper-complex models have been shown to be able to both capture these local relations better than real-valued models, but also to do so at a reduced parameter count due to their weight sharing property. However, as stated earlier, these models are constrained to two or four dimensions. Below we detail the work done showing how hyper-complex models capture these local features as well as the motivation to generalize them to any number of dimensions.

Consider the most common method for representing an image, which is by using three 2D matrices where each matrix corresponds to a color channel. Traditional real-valued networks treat this input as a group of unidimensional elements that may be related to one another, but not only does it need to try to learn that relation, it also needs to try to learn global features such as edges and shapes. By encoding the color channels into a

---

<sup>1</sup>The full code is available at <https://github.com/gaudetcj/VectorMapConv>

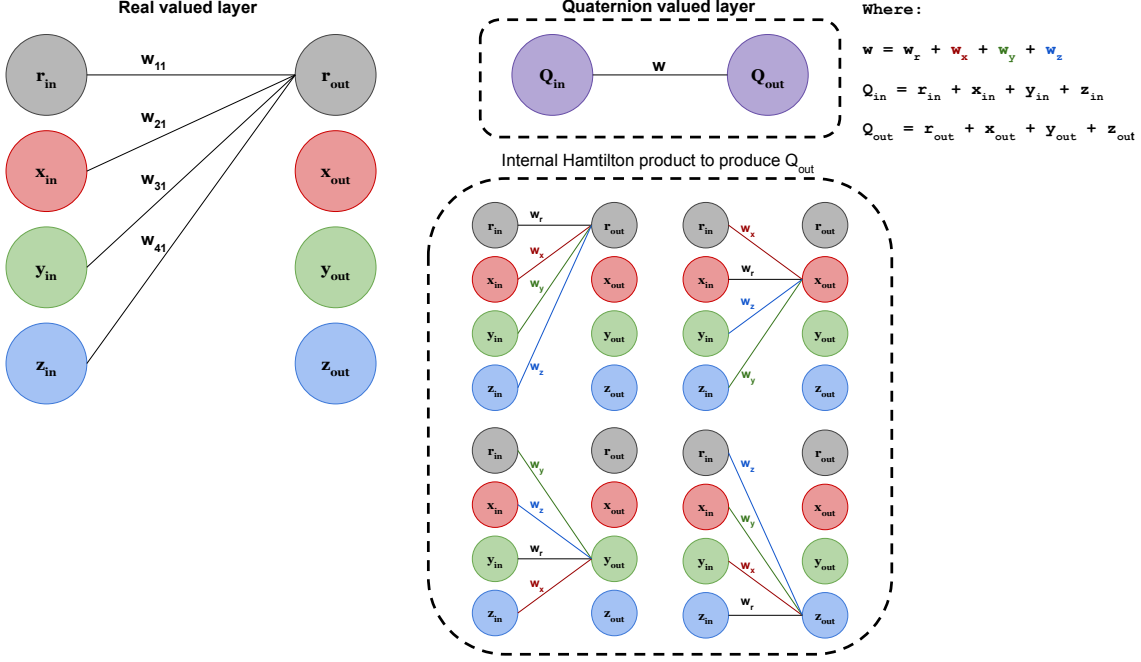


Figure 1: Illustration of the difference between a real-valued layer (left) and quaternion-valued layer (right). The quaternion’s Hamilton product shows the internal relation learning ability not present in the real-valued. Weight sharing occurs because the same set of weights is used in four outputs.

quaternion, each pixel is treated as a whole entity whose color components are strongly related. It has been shown that the quaternion algebra is responsible for allowing QNNs to capture these local relations. For example, Parcollet et al. [16] showed that a real-valued, encoder-decoder fails to reconstruct unseen color images due to it failing to capture local (color) and global (edges and shapes) features independently, while the quaternion encoder-decoder can do so. Their conclusion is that the Hamilton product of the quaternion algebra allows the quaternion network to encode the color relation since it treats the colors as a single entity. The Hamilton product forces a different linear combination of the internal elements to create each output element. This is seen in Fig. 1 from [18], which shows how a real-valued model looks when converted to a quaternion model. Notice that the real-valued model treats local and global weights at the same level, while the quaternion model learns these local relations during the Hamilton product. The weight sharing property can also be seen where each element of the weight is used four times, reducing the parameter count by a factor of four from the real-valued model.

The advantages of hyper-complex networks on multidimensional data seems

clear, but what about niche cases where there are higher dimensions than four? Examples include applications where one needs to ingest extra channels of information in addition to RGB for image processing, like satellite images which have several bands. To overcome this limitation we introduce vector map convolutions, which attempt to generalize the benefits of hyper-complex networks to any number of dimensions. We also add a learnable set of parameters that modify the linear combination of internal elements to allow the model to decide how important each dimension may be in calculating others.

### 3 Vector Map Components

This section will include the work done to obtain a working vector map network. This includes the vector map convolution operation and the weight initialization used.

#### 3.1 Vector Map Convolution

Vector map convolutions use a similar mechanism to that of complex [25] and quaternion [5] convolutions but in a more general way that does not bind it to a hyper-complex algebra. We will begin by observing the quaternion valued layer from Fig. 1. Our goal is to capture the properties of weight sharing and each output axis being composed of a linear combination of all the input axes, but for an arbitrary number of dimensions  $D_{\text{vm}}$ .

For the derivation we will choose  $D_{\text{vm}} = N$ . Let  $V_{in}^n = [v_1, v_2, \dots, v_n]$  be an  $N$  dimensional input vector and  $W^n = [w_1, w_2, \dots, w_n]$  be an  $N$  dimensional weight vector. Note that for the complex and quaternion case the output vector is a set of different linear combinations where each input vector is multiplied by each weight vector element a total of one time over the set. To achieve a similar result we will define a permutation function:

$$\tau(v_i) = \begin{cases} v_n & i = 1 \\ v_{i-1} & i > 1. \end{cases}$$

By applying  $\tau$  to each element in  $V^n$  a new vector is created that is a

circular right shifted permutation of  $V^n$ :

$$\tau(V^n) = [v_n, v_1, v_2, \dots, v_{n-1}].$$

Let the repeated composition of  $\tau$  be denoted as  $\tau^n$ , then we can define the resultant output vector  $V_{out}$  as:

$$V_{out}^n = [W^n \cdot V_{in}^n, \tau^2(W^n) \cdot V_{in}^n, \dots, \tau^{n-2}(W^n) \cdot V_{in}^n, \tau^{n-1}(W^n) \cdot V_{in}^n] \quad (1)$$

where  $|\cdot|$  is the dot product of the vectors. The above gives each element of  $V_{out}^n$  a unique linear combination of the elements of  $V_{in}^n$  and  $W^n$  since we never need to compose  $\tau$  above  $n - 1$  times (meaning the original vector  $W^n$  and any permutation only appear once).

The previous discussion applies to densely connected layers. The same idea is easily mapped to convolutional layers where the elements of  $V_{in}^n$  and  $W^n$  are matrices. To develop intuitions, the quaternion convolution operation is depicted in Fig. 2. The top of the figure shows four multichannel inputs and four multichannel kernels to be convolved. The resulting output is shown at the bottom of the figure. Each row in the middle of the figure shows the calculation of one output feature map, which is a ‘convolutional’ linear combination of one feature map with the four kernels (and the kernel coefficients are distinct for each row). When looking at the pattern across the rows, the weight sharing can be seen. Across the rows, any given kernel is convolved with four different feature maps. The only thing constraining the dimension to four is the coefficient values at the bottom of the figure imposed by the quaternion algebra (for more detail, see [5]). We hypothesize that the only thing important about the coefficient values is how they constrain the linear combinations to be independent. We also propose that the circularly shifted permutations just described generate admissible linear combinations. In this case, space permitting, Fig. 2 could be a  $5 \times 5$  image, where five filters are convolved with five feature maps while the weight sharing properties are preserved. That, is there is no longer a dimensional constraint.

We also define a learnable constant defined as a matrix  $\mathbf{L} \in \mathbb{R}^{D_{vm} \times D_{vm}}$ :

$$l_{i,j} = \begin{cases} 1 & i = 1 \\ 1 & i = j \\ 1 & j = (i + (i - 1)) \\ -1 & else. \end{cases}$$

The purpose of this matrix is to perform scalar multiplication with the input matrix, which will allow the network some control over how much the value of one axis influences another axis (the resultant axes all being different linear combinations of each axis).

With all of the above we can look at an example where  $D_{\text{vm}} = 4$  so we can then compare to the quaternion convolution. Here we let the weight filter matrix  $\mathbf{W} = [\mathbf{A}, \mathbf{B}, \mathbf{C}, \mathbf{D}]$  by an input vector  $\mathbf{h} = [\mathbf{w}, \mathbf{x}, \mathbf{y}, \mathbf{z}]$

$$\begin{bmatrix} \mathcal{R}(\mathbf{W} * \mathbf{h}) \\ \mathcal{I}(\mathbf{W} * \mathbf{h}) \\ \mathcal{J}(\mathbf{W} * \mathbf{h}) \\ \mathcal{K}(\mathbf{W} * \mathbf{h}) \end{bmatrix} = \mathbf{L} \odot \begin{bmatrix} \mathbf{A} & \mathbf{B} & \mathbf{C} & \mathbf{D} \\ \mathbf{D} & \mathbf{A} & \mathbf{B} & \mathbf{C} \\ \mathbf{C} & \mathbf{D} & \mathbf{A} & \mathbf{B} \\ \mathbf{B} & \mathbf{C} & \mathbf{D} & \mathbf{A} \end{bmatrix} * \begin{bmatrix} \mathbf{w} \\ \mathbf{x} \\ \mathbf{y} \\ \mathbf{z} \end{bmatrix} \quad (2)$$

where

$$\mathbf{L} = \begin{bmatrix} 1 & 1 & 1 & 1 \\ -1 & 1 & 1 & -1 \\ 1 & -1 & 1 & -1 \\ -1 & -1 & 1 & 1 \end{bmatrix} \quad (3)$$

The operator  $|\odot|$  denotes element-wise multiply. The sixteen parameters within  $\mathbf{L}$  are the initial values. They are otherwise unconstrained scalars and intended to be learnable. Thus, the vector map convolution is a generalization of complex, quaternion, or octonion convolution as the case may be, but it also drops the constraints imposed by the associated hyper-complex algebra.

For comparison the result of convolving a quaternion filter matrix  $\mathbf{W} = \mathbf{A} + i\mathbf{B} + j\mathbf{C} + k\mathbf{D}$  by a quaternion vector  $\mathbf{h} = \mathbf{w} + i\mathbf{x} + j\mathbf{y} + k\mathbf{z}$  is another quaternion,

$$\begin{bmatrix} \mathcal{R}(\mathbf{W} * \mathbf{h}) \\ \mathcal{I}(\mathbf{W} * \mathbf{h}) \\ \mathcal{J}(\mathbf{W} * \mathbf{h}) \\ \mathcal{K}(\mathbf{W} * \mathbf{h}) \end{bmatrix} = \begin{bmatrix} \mathbf{A} & -\mathbf{B} & -\mathbf{C} & -\mathbf{D} \\ \mathbf{B} & \mathbf{A} & -\mathbf{D} & \mathbf{C} \\ \mathbf{C} & \mathbf{D} & \mathbf{A} & -\mathbf{B} \\ \mathbf{D} & -\mathbf{C} & \mathbf{B} & \mathbf{A} \end{bmatrix} * \begin{bmatrix} \mathbf{w} \\ \mathbf{x} \\ \mathbf{y} \\ \mathbf{z} \end{bmatrix}, \quad (4)$$

where  $\mathbf{A}$ ,  $\mathbf{B}$ ,  $\mathbf{C}$ , and  $\mathbf{D}$  are real-valued matrices and  $\mathbf{w}$ ,  $\mathbf{x}$ ,  $\mathbf{y}$ , and  $\mathbf{z}$  are real-valued vectors. See Fig. 2 for a visualization of the above operation. More explanation is given in [5].

The question arises whether the empirical improvements observed in the use of complex and quaternion deep networks are best explained by the

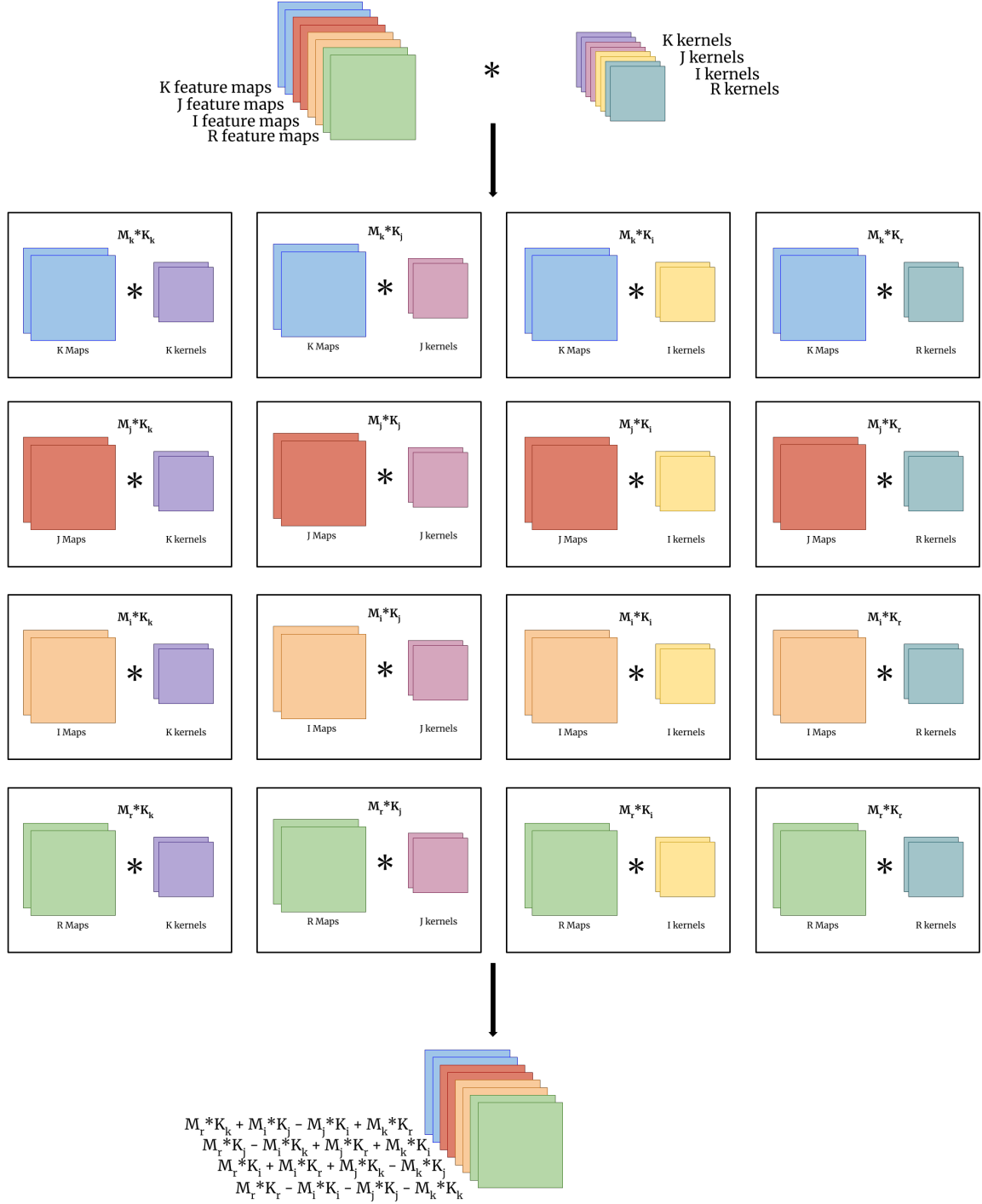


Figure 2: An illustration of quaternion convolution.



full structure of the hyper/complex algebra, or whether the weight sharing underlying the generalized convolution is responsible for the improvement.

### 3.2 Vector Map Weight Initialization

Proper initialization of the weights has been shown to be vital to convergence of deep networks. The weight initialization for vector map networks uses the same procedure seen in both deep complex networks [25] and deep quaternion networks [5]. In both cases, the expected value of  $|W|^2$  is needed to calculate the variance:

$$\mathbb{E}[|W|^2] = \int_{-\infty}^{\infty} x^2 f(x) dx \quad (5)$$

where  $f(x)$  is a multidimensional independent normal distribution where the number of degrees of freedom is two for complex and four for hyper-complex. Solving Eq. 5 gives  $2\sigma^2$  for complex and  $4\sigma^2$  for quaternions. Indeed, when solving Eq. 5 for a multidimensional independent normal distribution where the number of degrees of freedom is  $D_{\text{vm}}$ , the solution will equal  $D_{\text{vm}}\sigma^2$ . Therefore, in order to respect the Glorot and Bengio [6] criteria, the variance would be equal to :

$$\sigma = \sqrt{\frac{2}{D_{\text{vm}}(n_{\text{in}} + n_{\text{out}})}} \quad (6)$$

and in order to respect the He [8] criteria, the variance would be equal to:

$$\sigma = \sqrt{\frac{2}{D_{\text{vm}}n_{\text{in}}}}. \quad (7)$$

This is used alongside a vector of dimension  $D_{\text{vm}}$  that is generated following a uniform distribution in the interval  $[0, 1]$  and then normalized. The linear combination parameter  $\mathbf{L}$  in Eq. 2 is simply generated by randomly selecting from the set  $\{-1, 1\}$ .

## 4 Experiments and Results

We perform three sets of experiments designed to see baseline performance, compare against some known quaternion results, and to test extreme cases

of dimensionality in the data. This is done by simple classification on CIFAR data using different size ResNet models for real, quaternion, and vector map. The second experiment replicates the results of colorizing images using a convolutional auto-encoder from [16], but using vector map convolution layers. Lastly, the DSTL Satellite segmentation challenge from Kaggle [1] is used to demonstrate the high parameter count reduction when vector map layers are used for high dimensional data.

## 4.1 CIFAR Classification

### 4.1.1 CIFAR Methods

These experiments cover simple image classification using CIFAR-10 and CIFAR-100 datasets [11]. The CIFAR datasets are  $32 \times 32$  color images of 10 and 100 classes respectively. Each image contains only one class and labels are provided. Since the CIFAR images are RGB, we use  $D_{\text{vm}} = 3$  for all the experiments.

For the architecture we use different Residual Networks taken directly from the original paper [7]. We ran direct comparisons between real-valued, quaternion, and vector map networks on three different sizes: ReNet18, ResNet34, and ResNet50. The only change from the real-valued to vector map networks is that the number of filters at each layer is changed such that the parameter count is roughly the same as the real-valued network.

### 4.1.2 CIFAR Results

The results are shown in Table 1 as well as the validation loss and accuracy plots shown in Fig. 3. Also shown in Fig. 4 is the histogram of  $\mathbf{L}$  for the ResNet18 vector map convolution network. We note that they appear to be normally distributed around the initial values of either -1 or 1. We also include some visualizations of feature vector maps from the first convolution channel randomly selected on a few images in Fig. 5 of the vector map model.

The vector map network’s final accuracy outperforms the other models in all cases except one and the accuracy rises faster than both the real and quaternion valued networks. This may be due to the ability to control the

Architecture	Params	CIFAR-10	CIFAR-100
ResNet18 Real	11,173,962	5.92	27.81
ResNet18 Quaternion	8,569,242	5.92	28.77
ResNet18 Vector Map	7,376,320	6.05	27.18
ResNet34 Real	21,282,122	5.73	28.18
ResNet34 Quaternion	16,315,610	5.73	27.24
ResNet34 Vector Map	14,044,960	5.55	25.88
ResNet50 Real	23,520,842	6.10	27.40
ResNet50 Quaternion	18,080,282	6.10	27.32
ResNet50 Vector Map	15,559,120	5.72	25.16

Table 1: Percent error for classification on CIFAR-10 and CIFAR-100. Params is the total number of parameters.

relationships of each color channel in the convolution operation, while the quaternion is stuck to its set algebra, and the real is not combining the color channels in a similar fashion to either.

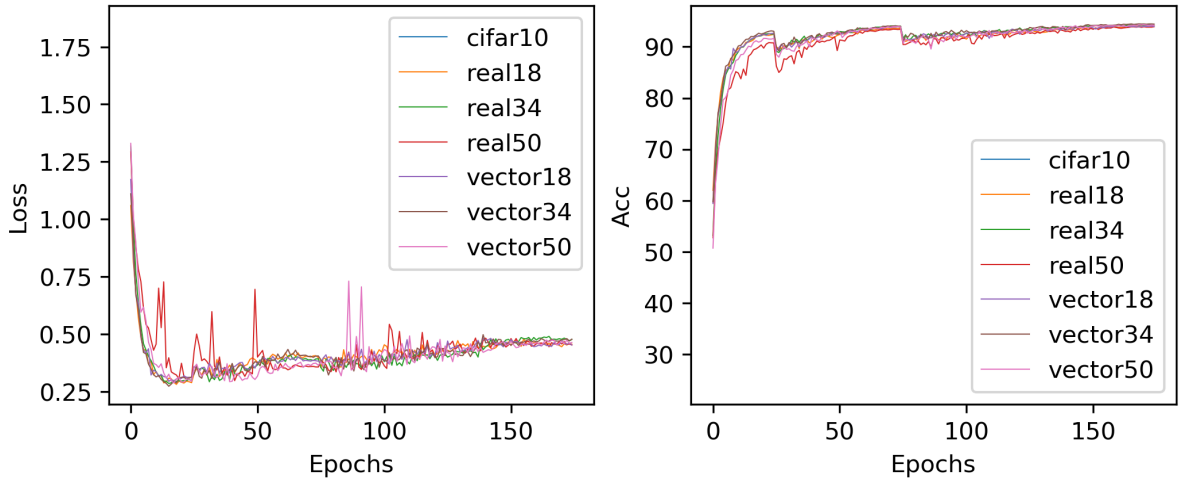


Figure 3: Validation loss and accuracy plots for CIFAR-10 corresponding to the experimental runs that produced Table 1.

## 4.2 CAE

### 4.2.1 CAE Methods

This experiment originally was to explore the power of quaternion networks over real-valued by investigating the impact the Hamilton product had on

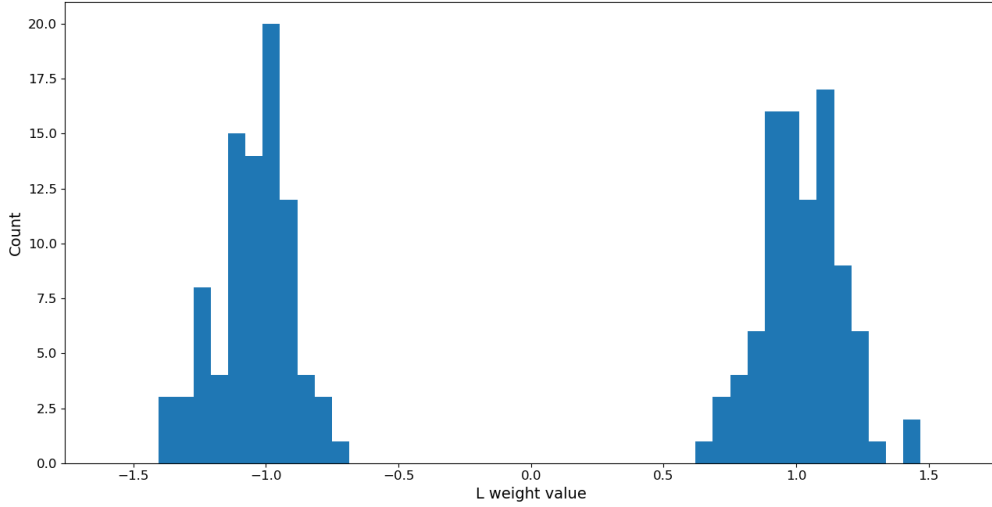


Figure 4: Histogram of  $\mathbf{L}$  values after training of the ResNet18 vector map convolution network.

reconstructing color images from gray-scale only training [16]. A convolutional encoder-decoder (CAE) was used to test color image reconstruction. We performed the exact same experiment using quaternions, but also two experiments using vector map layers with  $D_{\text{vm}} = 3$  and  $D_{\text{vm}} = 4$ . This way we can test if we mimic the quaternion results with four dimensions and if we are capturing the important components of treating the input dimensions as a single entity with three dimensions. The identical architecture is used, two convolutional encoding layers followed by two transposed convolutional decoding layers.

A single image is first chosen, then converted to gray-scale using the function  $GS(p_{x,y})$ , where  $p_{x,y}$  is the color pixel at location  $x, y$ . The gray value is concatenated three times for each pixel to create the input to the vector map CNN. We used the exact same model architecture, but since the output feature maps is three times larger in the vector map model we reduce their size to 10 and 20. The kernel size and strides are 3 and 2 for all layers. The model is trained for 3000 epochs using the Adam optimizer [10] using a learning rate of  $5e^{-4}$ . The weights are initialized following the above scheme and the hardtanh [4] activation function is used in both the convolutional and transposed convolutional layers.

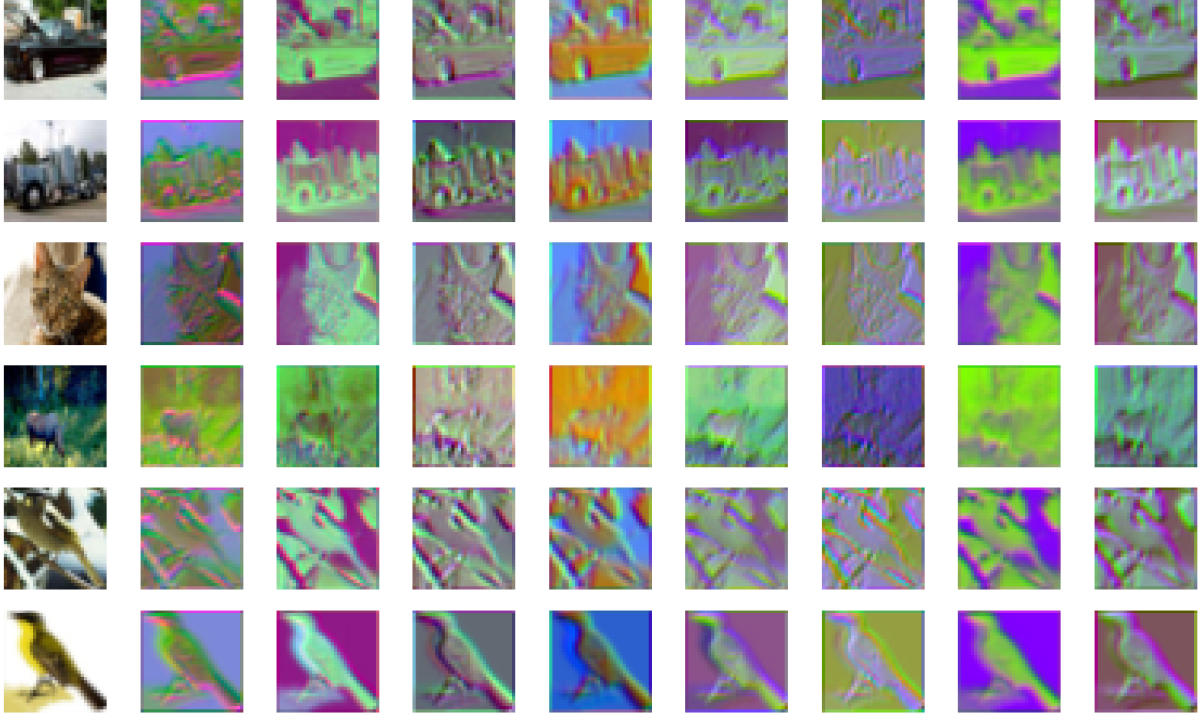


Figure 5: Randomly selected feature vector maps from the first convolution layer after training. Each row is a different image, where the first column are the original input images.

#### 4.2.2 CAE Results and Discussions

The results can be seen in Fig. 6 where one can see the vector map CAE was able to correctly produce color images like the quaternion CAE. Similar to the quaternion CAE, the vector map CAE appears to learn to preserve the internal relationship between the pixels similar to the Hamilton. The reconstructed images were also evaluated numerically using the peak signal to noise ratio (PSNR) [26] and the structural similarity (SSIM) [27]. These evaluations appear in Table 2.

Image	$D_{\text{vm}} = 3$ PSNR, SSIM	$D_{\text{vm}} = 4$ PSNR, SSIM	Quat PSNR, SSIM
kodim23	28.94dB, 0.97	29.14dB, 0.96	31.68dB, 0.96
kodim04	26.95dB, 0.96	26.99dB, 0.96	28.06dB, 0.93

Table 2: PSNR and SSIM results for vector map CAE compared to quaternion CAE.

The main goal of this experiment was to test if there exists a property of the quaternion structure that may have not been captured with the attempted generalization of vector map convolutions. Since both vector map networks perform similarly to the quaternion network it appears that the



Figure 6: Grey-scale to color results on two KODAK images for a quaternion CAE and a vector map CAE.

way the vector map rules are constructed enable it to capture the essence of the Hamilton product for any dimension size  $D_{\text{vm}}$  and the additional aspects of the algebraic structure are not important. Since the  $D_{\text{vm}} = 3$  model matched the quaternion performance, we have shown that the same performance can be achieved with fewer parameters.

### 4.3 DSTL

The Dstl Satellite Imagery Feature Detection challenge was run on Kaggle [1] where the goal was to segment 10 classes from 1km x 1km satellite images in both 3-band and 16-band formats. Since satellite images have many more bands of information than standard RGB, it makes it a good use case for vector map convolutions. We run experiments using the full bands on both real-valued and vector map networks.

### 4.4 DSTL Methods

Both models use a standard U-Net base as described in the original paper [21]. We use the entire 16-band format as input, simply concatenating them into one input to the models. For the vector map network we choose

$D_{\text{vm}} = 16$  to treat the entire 16-band input as a single entity. The real-valued model has a starting filter count of 32, while the vector map has a starting filter count of 96. The images are very large so we sample from them in sizes of 82 x 82 pixels, but only use the center 64 x 64 pixels for the prediction. For training, the batch size is set to 32, the learning rate is 1e-3, and we decay the learning rate by a factor of 10 every 25 epochs during a total of 75 epochs.

Some of the classes of the data set are only in a couple of images. Due to this reason, we train on all available images, but hold out random 400 x 400 chunks of the original images. We use the same seed for both the real-valued and vector map runs

## 4.5 DSTL Results

The results are shown in Table. 3 where one can see that for a lower parameter budget, the vector map achieved better segmentation performance. Some of the features, like the vegetation and water, stand out more distinctly in the non-RGB bands of information and the vector map seems to have captured this more accurately. The main goal was to show that the vector map convolutions could handle a large number of input dimensions and potentially better capture how the channels relate to one another.

Architecture	Params	Jaccard Score
UNet Real	7,855,434	0.427
UNet Vector Map	5,910,442	0.436

Table 3: Jaccard score on DSTL Satellite segmentation challenge for real-valued and vector map UNet models. Params is the total number of parameters.

## 5 Conclusions

This paper proposes vector map convolutions to generalize the beneficial properties of convolutional complex and hyper/complex networks to any number of dimensions. We also introduce a new learnable parameter to modify the linear combination of internal features.

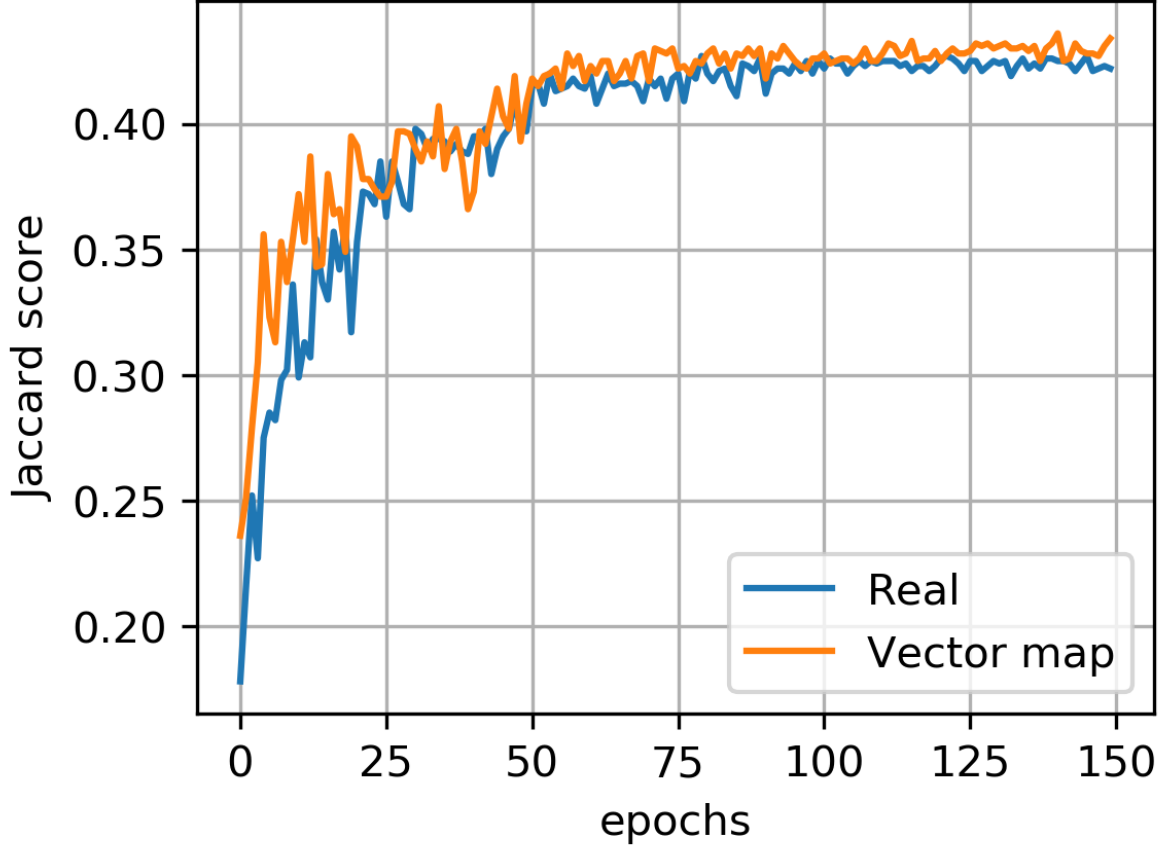


Figure 7: Validation loss using Jaccard score.

The first set of experiments compares performance of vector map convolutions against real-valued networks in three different sized ResNet models on CIFAR datasets. They demonstrate that vector map convolution networks have similar accuracy at a reduced parameter count effectively mimicking hyper-complex networks while consuming fewer resources. We also investigate the distribution of the final values of  $\mathbf{L}$ , the linear combination terms, and see that they also tend to stay around the value they were initialized to.

We further investigated if vector map convolutions effectively mimic quaternion convolution in its ability to capture color features more effectively with the Hamilton Product with image color reconstruction tests. The vector map convolution model not only can reconstruct color like the quaternion CAE, but it performs better as indicated by PSNR and SSIM measures. This shows that other aspects of the quaternion algebra are not relevant to this task and suggests that vector map convolutions could effectively capture the internal relation of any dimension input for different data types.



The final experiment tested the ability of vector map convolutions to perform well on very high dimensional input. We compared a real-valued model against a vector map model in the Kaggle DSTL satellite segmentation challenge dataset, which has 12 channels of image information and contains 10 classes. The vector map model was built with  $D_{\text{vm}} = 12$  and not only had fewer learnable parameters than the real-valued model, it achieved a higher Jaccard score and learned at a faster rate. This establishes advantage of vector map convolutions in higher dimensions.

This set of experiments have shown that vector map convolutions appear to not only capture all the benefits of complex/hyper-complex convolutions, but can outperform them using a smaller parameter budget while also being free from their dimensional constraints.

# References

- [1] Kaggle dstl satellite imagery feature detection. <https://www.kaggle.com/c/dstl-satellite-imagery-feature-detection>. Accessed: 2020-05-30.
- [2] Igor Aizenberg and Alexander Gonzalez. Image recognition using mlmvn and frequency domain features. In *2018 International Joint Conference on Neural Networks (IJCNN)*, pages 1–8. IEEE, 2018.
- [3] Eduardo Bayro-Corrochano, Luis Lechuga-Gutiérrez, and Marcela Garza-Burgos. Geometric techniques for robotics and hmi: Interpolation and haptics in conformal geometric algebra and control using quaternion spike neural networks. *Robotics and Autonomous Systems*, 104:72–84, 2018.
- [4] Ronan Collobert. Large scale machine learning. Technical report, IDIAP, 2004.
- [5] Chase J. Gaudet and Anthony S. Maida. Deep quatertion networks. In *2018 International Joint Conference on Neural Networks (IJCNN)*, 2018.
- [6] Xavier Glorot and Yoshua Bengio. Understanding the difficulty of training deep feedforward neural networks. In *Proceedings of the Thirteenth International Conference on Artificial Intelligence and Statistics*, pages 249–256, 2010.
- [7] Kaiming He, Xiangyu Zhang, Shaoqing Ren, and Jian Sun. Deep residual learning for image recognition. *arXiv preprint arXiv:1512.03385*, 2015.
- [8] Kaiming He, Xiangyu Zhang, Shaoqing Ren, and Jian Sun. Delving deep into rectifiers: Surpassing human-level performance on imagenet classification. In *Proceedings of the IEEE international conference on computer vision*, pages 1026–1034, 2015.
- [9] Teiji Isokawa, Tomoaki Kusakabe, Nobuyuki Matsui, and Ferdinand Peper. Quaternion neural network and its application. In *International conference on knowledge-based and intelligent information and engineering systems*, pages 318–324. Springer, 2003.
- [10] Diederik P Kingma and Jimmy Ba. Adam: A method for stochastic optimization. *arXiv preprint arXiv:1412.6980*, 2014.

- [11] Alex Krizhevsky and Geoffrey Hinton. Learning multiple layers of features from tiny images. 2009.
- [12] Hiromi Kusamichi, Teijiro Isokawa, Nobuyuki Matsui, Yuzo Ogawa, and Kazuaki Maeda. A new scheme for color night vision by quaternion neural network. In *Proceedings of the 2nd International Conference on Autonomous Robots and Agents*, volume 1315. Citeseer, 2004.
- [13] Nobuyuki Matsui, Teijiro Isokawa, Hiromi Kusamichi, Ferdinand Peper, and Haruhiko Nishimura. Quaternion neural network with geometrical operators. *Journal of Intelligent & Fuzzy Systems*, 15(3, 4):149–164, 2004.
- [14] Titouan Parcollet, Mohamed Morchid, and Georges Linares. Deep quaternion neural networks for spoken language understanding. In *2017 IEEE Automatic Speech Recognition and Understanding Workshop (ASRU)*, pages 504–511. IEEE, 2017.
- [15] Titouan Parcollet, Mohamed Morchid, and Georges Linares. Quaternion denoising encoder-decoder for theme identification of telephone conversations. 2017.
- [16] Titouan Parcollet, Mohamed Morchid, and Georges Linares. Quaternion convolutional neural networks for heterogeneous image processing. In *ICASSP 2019-2019 IEEE International Conference on Acoustics, Speech and Signal Processing (ICASSP)*, pages 8514–8518. IEEE, 2019.
- [17] Titouan Parcollet, Mohamed Morchid, and Georges Linares. A survey of quaternion neural networks. *Artificial Intelligence Review*, 53(4):2957–2982, 2020.
- [18] Titouan Parcollet, Mirco Ravanelli, Mohamed Morchid, Georges Linares, Chiheb Trabelsi, Renato De Mori, and Yoshua Bengio. Quaternion recurrent neural networks. *arXiv preprint arXiv:1806.04418*, 2018.
- [19] Titouan Parcollet, Ying Zhang, Mohamed Morchid, Chiheb Trabelsi, Georges Linares, Renato De Mori, and Yoshua Bengio. Quaternion convolutional neural networks for end-to-end automatic speech recognition. *arXiv preprint arXiv:1806.07789*, 2018.

- [20] Dario Pavllo, David Grangier, and Michael Auli. Quaternet: A quaternion-based recurrent model for human motion. *arXiv preprint arXiv:1805.06485*, 2018.
- [21] Olaf Ronneberger, Philipp Fischer, and Thomas Brox. U-net: Convolutional networks for biomedical image segmentation. In *International Conference on Medical image computing and computer-assisted intervention*, pages 234–241. Springer, 2015.
- [22] Kazuhiko Takahashi, Ayana Isaka, Tomoki Fudaba, and Masafumi Hashimoto. Remarks on quaternion neural network-based controller trained by feedback error learning. In *2017 IEEE/SICE International Symposium on System Integration (SII)*, pages 875–880. IEEE, 2017.
- [23] Keiichi Tokuda, Heiga Zen, and Tadashi Kitamura. Trajectory modeling based on hmms with the explicit relationship between static and dynamic features. In *Eighth European Conference on Speech Communication and Technology*, 2003.
- [24] C Trabelsi, O Bilaniuk, Y Zhang, D Serdyuk, S Subramanian, JF Santos, S Mehri, N Rostamzadeh, Y Bengio, and C Pal. Deep complex networks. arxiv 2018. *arXiv preprint arXiv:1705.09792*.
- [25] Chiheb Trabelsi, Olexa Bilaniuk, Ying Zhang, Dmitriy Serdyuk, Sandeep Subramanian, João Felipe Santos, Soroush Mehri, Negar Rostamzadeh, Yoshua Bengio, and Christopher Pal. Deep complex networks. In *International Conference on Learning Representations 2018 (Conference Track)*, 2018. arxiv:1705.09792.
- [26] Deepak S Turaga, Yingwei Chen, and Jorge Caviedes. No reference psnr estimation for compressed pictures. *Signal Processing: Image Communication*, 19(2):173–184, 2004.
- [27] Zhou Wang, Alan C Bovik, Hamid R Sheikh, and Eero P Simoncelli. Image quality assessment: from error visibility to structural similarity. *IEEE transactions on image processing*, 13(4):600–612, 2004.